

The Mass of Abell 1060 and AWM 7 from Spatially Resolved X-ray Spectroscopy: Variations in Baryon Fraction

M. Loewenstein¹ and R. F. Mushotzky

Laboratory for High Energy Astrophysics, NASA/GSFC, Code 662, Greenbelt, MD 20771

ABSTRACT

Using X-ray temperature and surface brightness profiles of the hot intracluster medium (ICM) derived from *ASCA* and *ROSAT* observations we place constraints on the dark matter (DM) and baryon fraction distributions in the poor clusters Abell 1060 (A1060) and AWM 7. Although their total mass distributions are similar, AWM 7 has twice the baryon fraction of A1060 in the best-fit models. The functional form of the DM distribution is ill-determined, however mass models where the baryon fractions in A1060 and AWM 7 significantly overlap are excluded. Such variations in baryon fraction are not predicted by standard models and imply that some mechanism in addition to gravity plays a major role in organizing matter on cluster scales.

Subject headings: cosmology: dark matter, galaxies: clusters: individual (AWM 7), galaxies: clusters: individual (Abell 1060)

1. Introduction

If gravity is the sole mechanism for organizing matter on large scales, then clusters of galaxies should share a common ratio of baryonic to nonbaryonic mass – that of the universe as a whole. Departures from such uniformity can be searched for using X-ray observations of the kind described in this paper; if such variations are discovered they provide direct evidence against the adequacy of standard cosmogenic scenarios. The poor clusters A1060 and AWM 7 comprise an excellent pair of objects for a study of this type. They are nearby, bright clusters of similar richness and X-ray temperature; however, AWM 7 is approximately five times more luminous in X-rays than A1060 (Edge & Stewart 1991). This suggests that the fraction of the total mass in baryons in AWM 7 is larger; this is confirmed by the detailed analysis of recent high quality X-ray data that follows.

¹Also with the Universities Space Research Association

2. ASCA Temperature Profiles

As required to constrain their DM distributions, accurate temperature profiles from *ASCA* spectra are available for A1060 and AWM 7. For A1060 we adopt the temperatures measured by Tamura 1996, while for AWM 7 the profile is obtained from archival performance verification phase data. Spectra were extracted in five annuli using standard screening and background subtraction procedures (e.g., Mushotzky et al. 1996), and fit with Raymond & Smith 1977 thermal plasma models using the XSPEC package. The observed profiles, with 90% confidence uncertainties, are shown in Figures 1a and 1b. The radial scale is computed for $H_o = 50 \text{ km s}^{-1} \text{ Mpc}^{-1}$, the value assumed throughout this paper.

The *ASCA* data have also been analyzed by Markevitch & Vikhlinin 1996, who derive an identical temperature profile and note the consistency with the *Einstein* MPC and *EXOSAT*. *HEAO-1* A2 (Schwartz et al. 1980) and *Ginga* (Tsuru 1993) large beam temperatures are consistent as well. Temperatures derived from *ROSAT* PSPC spectra are systematically lower by 20% (Neumann & Böhringer 1995, hereafter NB), perhaps due to small PSPC spectral calibration problems (Markevitch & Vikhlinin 1996). Our analysis is not sensitive to the cooling flow inside $\sim 2'$ detected with the PSPC.

Our temperature profiles do not account for the broad, energy-dependent wings of the *ASCA* point spread function (PSF), since any effect for these relatively cool clusters is small (Ohashi 1995). A comparison of our AWM 7 temperature profile with that of Markevitch & Vikhlinin 1996 and our own experience with PSF corrections indicates that our uncertainties may be underestimated by as much as a factor of 2. This is further supported by our analysis of AWM 7 that includes the effects of the *ASCA* PSF with software developed by Dr. K. A. Arnaud. For this reason we will be rather lenient in choosing acceptable mass models.

3. Models and Parameters

We derive DM distributions using the method of Loewenstein 1994 that produces physical, mathematically well-behaved temperature distributions based on an integration of the equation of hydrostatic equilibrium (HSE) inward from infinity. The consensus from numerical simulations of cluster formation (e.g., Navarro et al. 1995; Schindler 1996; Evrard et al. 1996) is that departures from HSE are generally small and mass estimation operating under the hydrostatic assumption accurate.

The total gravitating mass is assumed to consist of galaxy, gas, and nonbaryonic components. (The DM is assumed to be entirely nonbaryonic; any contribution from MACHOs would increase the inferred baryon fractions.) The baryonic parameters are based on optical and X-ray observations, while the DM distribution is parameterized by a scale-length and normalization. The two DM parameters and the pressure at infinity are varied until the model temperature

distribution, appropriately averaged and projected, matches the profile derived from *ASCA* spectra. A model is deemed acceptable if it predicts temperatures within $3\times$ the 90% uncertainties of the best-fits to the data in each annulus. The temperature in these models can take on arbitrary values outside of the limited *ASCA* field-of-view. We eliminate models where the temperature climbs to extreme values just outside the observed region by rejecting pressure-dominated models where the boundary pressure at the virial radius, r_{vir} , exceeds the average inside r_{vir} calculated using the mass-weighted temperature in the observed region.

This procedure for constraining the DM distribution effectively accounts for systematic uncertainties in the mass model from projection effects and limited spatial resolution and field-of-view. Because of the superb accuracy of PSPC surface brightness profiles and *ASCA* temperatures these effects dominate any statistical uncertainties.

The gas density distribution is modeled using the ‘ β model’ – $\rho_{gas} = \rho_{gas,o}(1 + r^2/a_{gas}^2)^{-1.5\beta}$, the galaxy distribution as the sum of two ‘King profiles’ – $\rho_{gal} + \rho_{cd} = \rho_{gal,o}(1 + r^2/a_{gal}^2)^{-1.5} + \rho_{cd,o}(1 + r^2/a_{cd}^2)^{-1.5}$ – to account for both central galaxy and smoothed cluster galaxy components. Our standard model for the DM distribution uses the function proposed by Navarro et al. 1995 that is an excellent characterization for a wide range of cluster formation scenarios (Cole & Lacey 1996, hereafter CL),

$$\rho_{dark} = \rho_{dark,o}(a_{dark}/r)(1 + r/a_{dark})^{-\alpha} \quad (1)$$

with $\alpha = 2$, although we have also experimented with other functional forms.

Our fixed, baryonic model parameters are displayed in Table 1. For AWM 7 we use the β model parameters from NB that we have confirmed using archival PSPC and *ASCA* data, and include the central cooling flow excess. The galaxy parameters are taken from Fujita & Kodama 1995 – their integrated optical luminosity agrees well with Beers et al. 1984 and Dell’Antonio et al. 1995. For A1060 the β model parameters are based on our own best-fit to the 0.4-2.0 keV PSPC surface brightness profile extracted from archival data. Galaxy parameters for A1060 are derived from de Vaucouleurs model fits to the light profiles of the overall cluster (Fitchett & Merritt 1988) and central galaxy (Vasterberg 1991), converting from de Vaucouleurs radius to King model core

Table 1. Gas And Galaxy Mass Distribution Parameters

Cluster	a_{gas}	$\rho_{gas,o}$	β	a_{gal}	$\rho_{gal,o}$	a_{cd}	$\rho_{cd,o}$
A1060	94	9.5	0.61	160	5.5	2.6	$8.6 \cdot 10^4$
AWM 7 ^a	102	13.	0.53	190	5.0	2.0	$3.0 \cdot 10^5$

radius by dividing by 12, and normalizing according to the luminosities in Edge & Stewart 1991 and Vasterberg 1991. We assume mass-to-light ratios, in solar units, of 5 in the visual band and 7 in the blue.

4. Results and Discussion

4.1. Baryon Fractions in Acceptable Mass Models

Figures 1a and 1b show projected, emission-averaged model temperature distributions superimposed on the *ASCA* temperatures for A1060 and AWM 7. The solid lines are the distributions for the best-fit mass models, the dotted lines the distributions with the most compact DM density profiles that meet the acceptance criterion, and the dashed lines those with the most diffuse DM distributions. The corresponding baryon fraction distributions as a function of radius in units of r_{vir} are shown in Figure 2. We have defined r_{vir} , following CL, as the radius within which the average overdensity is 178: 2 ± 0.5 Mpc for A1060, and 2 ± 0.4 Mpc for AWM 7. From $0.1r_{vir}$ to r_{vir} the baryon fraction distributions are flat, with a maximum increase of ≈ 2 over this decade in both clusters; there may be a modest decline for A1060. Despite spreading beyond the radius of the last temperature measurement ($\sim 0.25r_{vir}$), the observationally allowed baryon fraction distributions are disjoint at all $r > 0.05r_{vir}$. Total masses and baryon fractions within 0.5, 1, and 2 Mpc are displayed in Table 2. For the best-fit models the total mass distributions in the two clusters are very similar, but AWM 7 has twice the baryon fraction. Galaxies account for $\sim 40, 30,$ and 20% of the baryons within 0.5, 1, and 2 Mpc in A1060; the corresponding ratios in AWM 7 are $\sim 30, 20,$ and 10% : the ratio of stars to gas falls with radius in both clusters. Since abundances and optical luminosities are comparable, the ratio of intracluster (IC) metals to optical light is about twice as high in AWM 7.

4.2. Issues of Concern

NB derive an acceptable range of baryon fraction in AWM 7 of 0.11-0.27 at 1.2 Mpc: the lower limit is significantly less than in any of our allowed models at ~ 1 Mpc (Figure 2, Table 2). Examination of their Figure 6 reveals that the cause of the discrepancy is the sudden increase in the upper envelope of their permitted mass profiles for $r > 1$ Mpc. Such models with arbitrary mass profile shapes are allowed in NB, but not in our work: we assume that the DM can be characterized by a single smooth function out to r_{vir} (CL). The baryon fractions in NB are in good agreement with ours inside 1 Mpc.

Although we include the departure from the β model resulting from the cooling flow in AWM 7, we do not account for the likely complex thermal structure. Therefore, our derived baryon fractions inside $\sim r_{vir}/30$ may not be reliable in this cluster. Baryon fractions may be

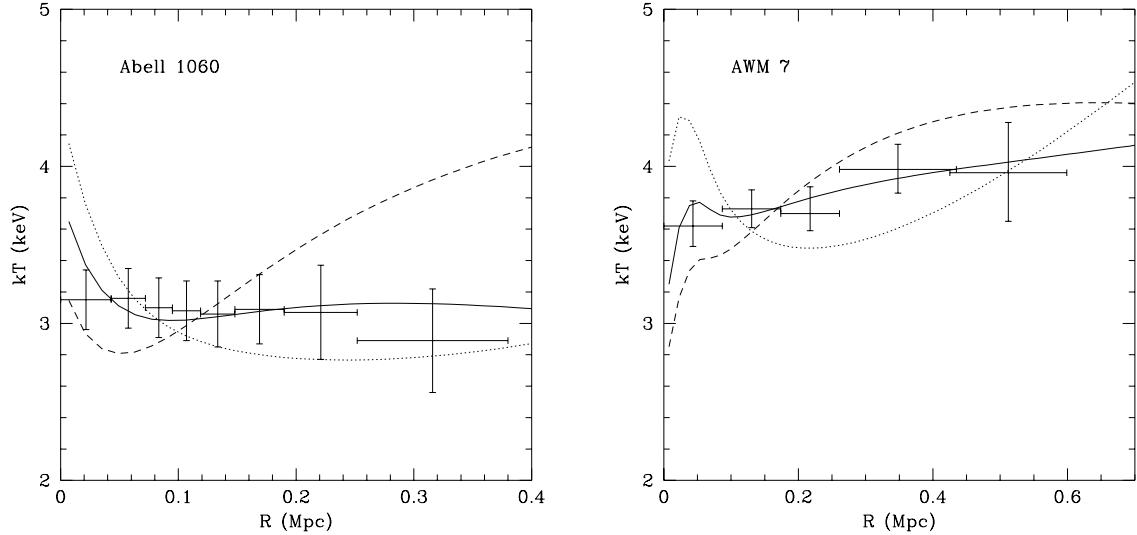


Fig. 1.— (a) Projected, emission-averaged model temperature distribution superimposed on the 90% confidence limits from *ASCA* (error bars) for A1060. The solid line indicates the best-fit mass model – $a_{dark} = 325$ kpc; the dotted (dashed) line the most compact (diffuse) acceptable mass model – $a_{dark} = 150$ (900) kpc. (b) Same as (1) but for AWM 7 with $a_{dark} = 300$, 100, and 650 kpc for the best-fit, most compact, and most diffuse dark matter models, respectively.

Table 2. Total Masses And Baryon Fractions

Cluster	a_{dark}/r_{vir} ^a	$M(0.5)$ ^b	$M(1.0)$	$M(2.0)$	$f(0.5)$ ^c	$f(1.0)$	$f(2.0)$
A1060	0.17(0.09-0.36)	1.0(0.80-1.1)	2.1(1.4-2.9)	3.6(2.2-6.3)	12(11-16)	13(9-19)	15(9-25)
AWM 7	0.15(0.06-0.29)	1.0(0.84-1.1)	2.1(1.5-2.6)	4.0(2.7-5.5)	21(20-26)	25(21-36)	33(25-50)

Note. — Best-fit model total masses M and baryon fractions f evaluated within 0.5, 1.0, and 2.0 Mpc, with allowed range in parentheses.

^aRatio of dark matter scale length to virial radius.

^bMasses in units of $10^{14} M_{\odot}$.

^cBaryon fractions in percent.

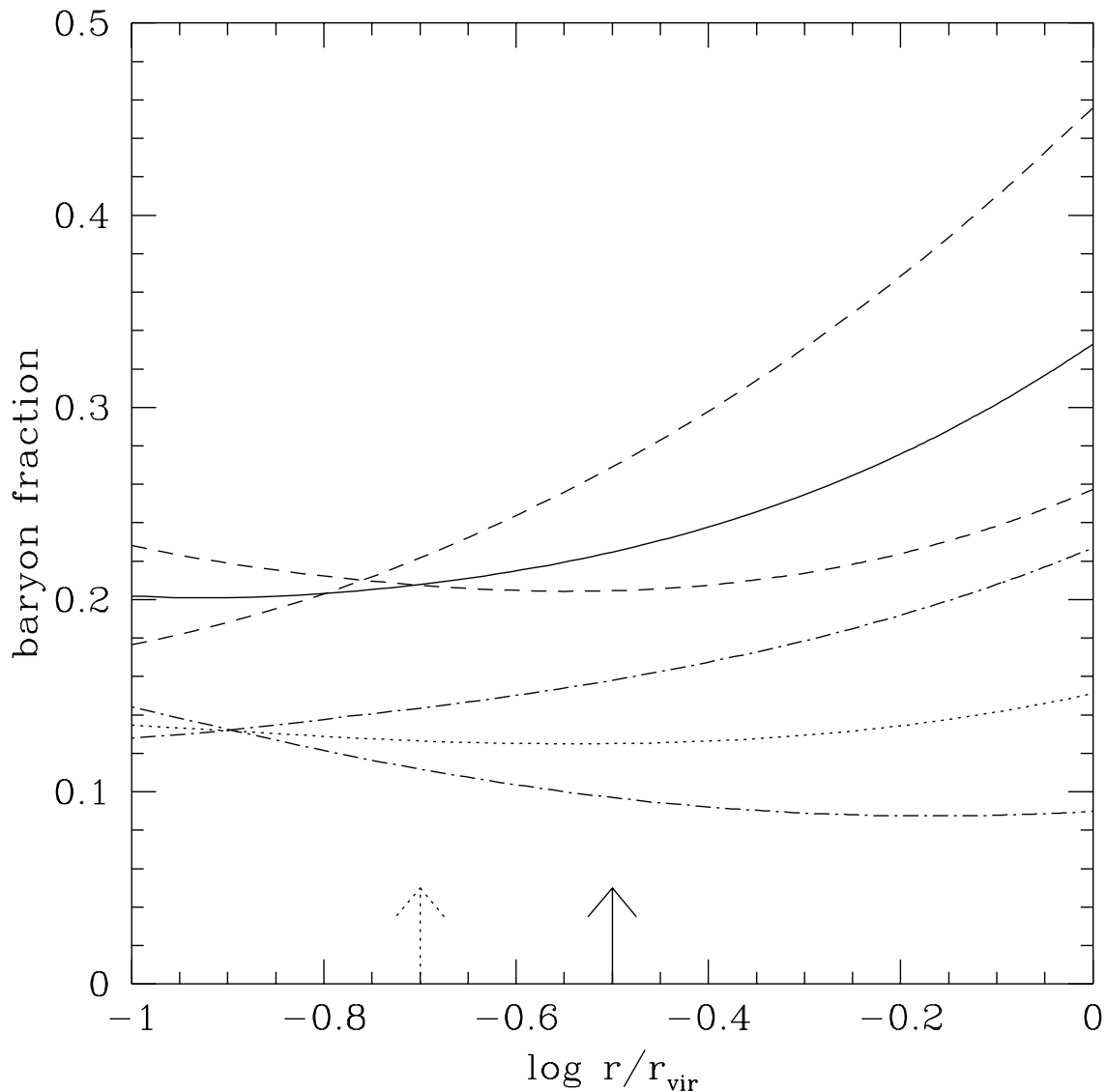


Fig. 2.— Enclosed baryon fractions vs. radius in units of the virial radius in A1060 and AWM 7. The dotted (solid) line represents the best-fit mass model, the dot-dashed (dashed) lines the most compact and diffuse models for A1060 (AWM 7). The compact models lie below the best fits. Arrows at the bottom of the plot show the approximate positions of the outermost radii where *ASCA* temperatures have been obtained.

overestimated by as much as a factor of 2 in a multi-phase ICM (Gunn & Thomas 1996). However, neither multi-temperature fits to the *ASCA* spectra nor examination of the ratio of He-like to H-like Fe K lines reveal any evidence for multiple temperatures in AWM 7 outside of the cooling flow region, with a maximum contribution (at 90% confidence) from gas hotter than 6 keV of 20%.

Finally, our assumption of circular symmetry cannot account for the baryon fraction discrepancy between A1060 and AWM 7 (White et al. 1994). If A1060 were prolate along the line-of-sight its baryon fraction might be *overestimated* (Daines et al. 1996); such a geometry is unlikely in the case of AWM 7 which appears elliptical in the plane of the sky.

4.3. The Form of the Dark Matter Distribution

X-ray observations of the ICM in A1060 and AWM 7 are well-explained using a mass model where DM follows the universal function (Equation 1 with $\alpha = 2$) predicted by numerical simulations of dissipationless hierarchical clustering in an $\Omega = 1$ universe with gaussian initial fluctuations. Furthermore, the constraints on the scale-lengths (a_{dark}/r_{vir} ; see Table 2) are consistent with cold dark matter numerical experiments – or other models with similar initial power spectra (Navarro et al. 1995; CL).

However, because of the limited spatial resolution and radial extent of the X-ray temperature profile, alternative DM density distributions are also allowed. DM models following Equation 1, but with $\alpha = 1$ or 3, can be constructed that provide fits to the data of comparable quality to the standard $\alpha = 2$ model. The acceptable $\alpha = 1$ ($\alpha = 3$) models have correspondingly smaller (larger) scale-lengths than their $\alpha = 2$ counterparts. Models with cores also prove acceptable: we cannot constrain the DM slope at small or large radii.

The inferred total mass within the outermost radii where the temperature has been measured using *ASCA* (380 kpc for A1060 and 610 kpc for AWM 7) is independent of the assumed DM density slope. However, if the DM distribution is steep in A1060 the extrapolated baryon fraction could increase significantly beyond 1 Mpc: in this case the baryon fractions in the acceptable models for A1060 and AWM 7 overlap for $r > 0.75r_{vir}$. If the DM slope were steep in A1060 but flat in AWM 7 this region of overlap could be extended inwards to $r > 0.6r_{vir}$. However, the baryon fraction distributions remain disjoint inside 1 Mpc and the discrepancy between the best-fit models is still a factor of 2 at all $r < r_{vir}$. The baryon fraction distribution for all acceptable mass models with $1 \leq \alpha \leq 3$ is fairly flat, with maximum increases from $0.1r_{vir}$ to r_{vir} of 2 and 3 for A1060 and AWM 7, respectively, and a maximum decline of a factor of 2 in A1060.

Finally we note that, regardless of the form of the DM distribution, the average projected total mass surface density is ~ 0.15 and ~ 0.09 gm cm^{-2} within 100 and 200 kpc for both clusters. This is well below the critical density for strong gravitational lensing; however, these nearby clusters do not belong to the class of extremely hot and luminous systems where giant arcs have been detected at moderate redshift.

4.4. Implications

We have been conservative in constraining the mass distributions in A1060 and AWM 7, since the models with the smallest DM scale-lengths require a substantial, fine-tuned boundary pressure to reproduce the nearly flat observed temperature profiles. Moreover, the temperatures in these models rise linearly with radius beyond ~ 500 kpc (*i.e.* just outside the *ASCA* field of view): behavior not observed in more distant clusters. Thus the upper limit curves in Figure 2 are likely to be overestimates (and may already be ruled out by temperature measurements at larger radii in AWM 7; NB, Ezawa et al. 1996), and the allowed range of baryon fractions in A1060 and AWM 7 even more disjoint.

The X-ray data for A1060 and AWM 7 are best characterized by models where the baryon fraction in AWM 7 is approximately twice that of A1060 at all radii from $0.05r_{vir}$ to r_{vir} – about what one would expect from a simple scaling based on their X-ray luminosities. Under conservative assumptions about the uncertainties and allowing for differences in the shape of their DM distributions, the baryon fractions in A1060 and AWM 7 are marginally consistent at $r \sim r_{vir}$, but are clearly distinct inside $\sim r_{vir}/3$. Although a wide range of baryon fractions can be found in the literature (e.g., White & Fabian), we believe this is the first cluster-to-cluster comparison to explore the uncertainties resulting from different possible DM configurations and to demonstrate the necessity of a range of cluster baryon fractions. To the extent that X-ray temperature is a measure of total mass (Evrard et al. 1996) the spread in X-ray luminosity and mass accretion rate (two indicators of baryon richness) at a given X-ray temperature also implies a range in baryon fraction (Fabian et al. 1994), although clusters must be individually analyzed to verify this.

In standard cluster formation models driven solely by gravitational instability there is no mechanism for separating baryons and DM. Variations in baryon fraction of the kind we are reporting thus require an additional process. The most likely candidate is feedback, in the form of powerful supernovae-driven galactic outflows, from star formation in young galaxies during the protocluster epoch. Analysis of *ASCA* spectra of a number of clusters indicates that, not only is such powerful energy injection plausible, but is required to account for measured ICM abundances of type II supernova products such as O and Si (Mushotzky et al. 1996, Loewenstein & Mushotzky 1996). In some clusters this energy input could have resulted in the ejection of substantial amounts of IC gas into intercluster space, thus reducing their baryon fractions. Variations in gas retention could result from variations in star formation efficiency, initial mass function, or differences in timing in the sense that in a less relaxed cluster mass loss is facilitated by the occurrence of star formation in previrialized subclusters with relatively small binding masses.

This mechanism should be less efficient for more massive clusters; and indeed, preliminary analysis using *ASCA* temperatures of hotter clusters shows a remarkable uniformity in baryon fraction (Mushotzky et al. 1995). This is also consistent with the large apparent baryon fraction variations in groups (Mulchaey et al. 1996) where, moreover, the spread in the ratio of gas to stars may indicate that this energy injection can have a negative feedback effect on subsequent galaxy

formation.

5. Summary and Conclusions: Beyond the Baryon Catastrophe

We have derived constraints on the DM and baryon fraction distributions in the poor clusters A1060 and AWM 7 using *ASCA* and *ROSAT* observations of their ICM. The data are consistent with mass models where the form and length-scale of the DM distribution is identical to that found in numerical simulations of cluster formation. However the spatial resolution and extent of the observed temperature profiles is not sufficient to rule out other DM models or determine whether the baryon fraction distribution is flat or increasing (or decreasing, in the case of A1060) with radius.

Although they have similar optical luminosities and total masses the total baryon fraction distributions in A1060 and AWM 7 are disjoint, with the X-ray data favoring models where AWM 7 is approximately twice as baryon rich as A1060 for $0.05r_{vir} < r < r_{vir}$. The data for these and other clusters is consistent with a universal baryon fraction of ~ 0.25 ($\Omega = 0.1 - 0.4$, given nucleosynthetic constraints on the overall baryon density), but requires the existence of some gasdynamical process to deplete the number of baryons in a fraction of relatively low-mass systems (poor clusters and groups). Feedback from galaxy formation is a likely candidate to provide such a mechanism and is indicated by cluster abundance studies. Variations in baryon fraction bring standard models of structure formation where $\Omega = 1$, standard Big Bang nucleosynthesis is assumed, and gravity is the sole mechanism for organizing matter, into further conflict with the observed universe.

We thank T. Tamura for providing us with the A1060 temperature profile, and K. Arnaud for making spectral analysis software that includes the effects of the *ASCA* PSF available to us and for feedback on the draft manuscript.

REFERENCES

- Beers, T. C., Geller, M. J., Huchra, J. P., Latham, D. W., & Davis, R. J. 1984, *ApJ*, 283, 33
- Cole, S. M., & Lacey, C. G. 1996, *MNRAS*, 281, 716
- Daines, S., Jones, C., Forman, W., & Tyson, A. 1996, preprint
- Dell’Antonio, I. P., Geller, M. J., & Fabricant, D. G. 1995, *AJ*, 110, 502
- Edge, A. C., & Stewart, G. C. 1991, *MNRAS*, 252, 428
- Evrard, A. E., Metzler, C. A., & Navarro, J. F. 1996, *ApJ*, in press
- Ezawa, H., Fukazawa, Y., Haiguang, X., Ikuchi, K., Makishima, K., Ohashi, T., Tamura, T., & Yamasaki, N. 1996, in *X-ray Imaging and Spectroscopy of Cosmic Plasmas*, ed. F. Makino (Tokyo: Univ. Academy Press), in press
- Fabian, A. C., Crawford, C. S., Edge, A. C., & Mushotzky, R. F. 1994, *MNRAS*, 267, 779
- Fitchett, M., & Merritt, D. 1988, *ApJ*, 335, 18
- Fujita, Y., & Kodama, H. 1995, *ApJ*, 452, 177
- Gunn, K. F., & Thomas, P. A. 1996, *MNRAS*, in press
- Loewenstein, M. 1994, *ApJ*, 431, 91
- Loewenstein, M., & Mushotzky, R. F. 1996, *ApJ*, in press
- Markevitch, M., & Vikhlinin, A. 1996, *ApJ*, submitted
- Mulchaey, J. S., Davis, D. S., Mushotzky, R. F., & Burstein, D. 1996, *ApJ*, 456, 80
- Mushotzky, R. F., Loewenstein, M., Arnaud, K. A., & Fukazawa, Y. 1995, in *Dark Matter*, ed. S. S. Holt & C. L. Bennett (New York: AIP), p. 231
- Mushotzky, R. F., Loewenstein, M., Arnaud, K. A., Tamura, T., Fukazawa, Y., Matsushita, K., Kikuchi, K., & Hatsukade, I. 1996, *ApJ*, in press
- Navarro, J. F., Frenk, C. S., & White, S. D. M. 1995, *MNRAS*, 275, 720
- Navarro, J. F., Frenk, C. S., & White, S. D. M. 1996, *ApJ*, 462, 563
- Neumann, D. M., & Böhringer, H. 1995, *A&A*. 301, 865 (NB)
- Ohashi, T. 1995, in *Dark Matter*, ed. S. S. Holt & C. L. Bennett (New York: AIP), p. 255
- Raymond, J. C., & Smith, B. W. 1977, *ApJS*, 35, 419

Schindler, S. 1996, *A&A*, 305, 858

Schwartz, D. A., Davis, M., Doxsey, R. E., Griffiths, R. E., Huchra, J., Johnston, M. D.,
Mushotzky, R. F., Swank, J., & Tonry, J. 1980, *ApJ*, 238, L53

Takahashi, T., Markevitch, M., Fukazawa, Y., Ikebe, Y., Ishisaki, Y., Kikuchi, K., Makishima, K.,
& Tawara, Y 1995, *ASCA Newsletter*, no. 3 (NASA/GSFC)

Tamura, T., Day, C. S. R., Fukazawa, Y., Hatsukade, I., Ikebe, Y., Makishima, K., Mushotzky, R.
F., Ohashi, T., Takenake, K., & Yamashita, K. 1996, *PASJ*, in press

Tsuru, T. 1993, Ph D. Thesis, University of Tokyo

Vasterberg, A. R., Jorsater, S., & Lindblad, P. O. 1991, *A&A*, 247, 335

White, D. A., & Fabian, A. C. 1995, *MNRAS*, 273, 72

White, D. A., Fabian, A. C., Allen, S. W., Edge, A. C., Crawford, C. S., Johnstone, R. M.,
Stewart, G. C., & Voges, W. 1994, *MNRAS*, 269, 589